ADVANCED ELECTRONIC MATERIALS
Open Access
www.advelectronicmat.de

Dry Laser-Induced Graphene Fractal-like ECG Electrodes

Yann Houeix, Denice Gerardo, Francisco J. Romero, Víctor Toral, Lidia Hernandez, Almudena Rivadeneyra, Encarnación Castillo, Diego P. Morales, and Noel Rodriguez*

Fractal-like geometries applied to biosignal-electrodes design show great potential for enhancing the signal acquisition of sensing systems. This study reports a novel approach for flexible, silver-free, and dry fractal-like electrodes based on Laser-Induced Graphene (LIG) obtained through laser photothermal processing of a commercial polyimide film. This one-step mask-less manufacturing process enables the simple fabrication of natural and optimized fractal-like shapes inspired by actual snowflake patterns. To ensure a reliable and standardized connection to the measurement unit, the electrodes are equipped with a snap terminal. The electrodes are structurally characterized using various techniques including Scanning Electron Microscopy (SEM), Raman spectroscopy, and X-ray Photoelectron Spectroscopy (XPS). By benchmarking the performance of these electrodes against Ag/AgCl wet commercial electrodes and LIG electrodes shaped as commercial ones, a heart rate-monitoring accuracy of over 96.8% is achieved, with high specificity, positive prediction, and sensitivity, surpassing the 95.8% achieved by conventional commercial electrodes. These results demonstrate the efficacy of fractal-based designs in combination with LIG-based transduction, offering flexible and cost-effective electrocardiogram (ECG) electrodes with improved performance compared to traditional wet electrodes.

1. Introduction

Cardiovascular diseases (CVDs) are the leading cause of death worldwide, prompting significant efforts to enhance early diagnosis, prevention, and treatment.[1] Electrocardiography (ECG) is the most common technique to diagnose abnormal cardiac activity and extract information from the electrical signals generated by the heart, potentially enabling the preventive detection of CVDs.[2] In the last decades, with the advent of the Internet of Things (IoT) and wearable electronics, the diagnostic measurement of ECG signals is extending from hospital to home-care environments.[3–6] As the sensing component, the electrode plays a crucial role in ECG signal measurement. Ag/AgCl electrodes are the most commonly used bioelectrodes in cardiology, which are usually combined with a gel containing KCl electrolyte to decrease the skin-electrode contact impedance and reduce motion artifacts.[7] However, this type of electrodes present some issues. While they are cost-effective for large volume production, the gel applied to the skin can accumulate sweat and potentially cause discomfort during long-term ECG monitoring. Additionally, the gel dehydrates over time, leading to performance degradation and reduced flexibility of the electrode.[8,9] Because of that, dry electrodes have emerged as a potential alternative to conventional wet electrodes for ECG measurements, which has led to the investigation of multiple alternatives, including invasive microneedle electrodes, capacitive electrodes, and surface electrodes.[10,11]

More recently, flexible and wearable-oriented dry electrodes utilizing carbon-based conductive materials are attracting increasing attention. These materials include graphene,[12,13] carbon nanotubes (CNT),[14,15] or reduced Graphene Oxide (rGO).[16] Among the carbon-based materials, Laser-Induced Graphene (LIG) stands out due to its high electrical conductivity, mechanical flexibility, simplicity of production, scalability, and low cost; as it features a one step manufacturing process compatible with roll-to-roll processes.[17] Previous studies have already demonstrated the potential of LIG in ECG monitoring, reporting promising results.[18–21] However, most of the previous designs and commercial electrodes have been constrained to fixed transduction areas, commonly adopting a typical circular shape with ≈10 mm of diameter, therefore missing the potential offered by Direct Laser Writing (DLW) techniques in exploring more complex patterns, such as fractal-like geometries, without the need for complex lithographic processes.

The application of fractal-like structures has been reported in various fields, including stretchable electronics,[22] neuron electrodes,[23] gas sensors,[24] and antennas.[25] Fractal

Y. Houeix, D. Gerardo, F. J. Romero, V. Toral, A. Rivadeneyra, E. Castillo, D. P. Morales, N. Rodriguez
Dept. Electronics and Computer Technology
Faculty of Sciences
University of Granada
Granada 18071, Spain
E-mail: franromero@ugr.es

D. Gerardo, L. Hernandez
Facultad de Biología
Universidad Autónoma de Sinaloa
Culiacán 80040, México

The ORCID identification number(s) for the author(s) of this article can be found under https://doi.org/10.1002/aelm.202300767

DOI: 10.1002/aelm.202300767

ADVANCED ELECTRONIC MATERIALS Open Access
www.advelectronicmat.de

geometries possess a set of features that set them apart from traditional Euclidean geometries.[26,27] These structures exhibit self-similarity, whereby each component of the structure resembles a scaled-down replica of the entire structure. Unlike regular geometries, fractal geometries do not have a finite characteristic length. Instead, the length increases as the scale unit used to measure the geometry decreases, accounting for more accurate details.[28] A well-known natural example of 2D fractal geometries are the snowflakes, which exhibit a fractal dimension ranging from 1.4 to 2.[29,30] Snowflakes are formed from frozen water vapor in the atmosphere, developing a unique hexagonal crystal lattice structure with self-similarity and a high degree of symmetry as they grow.[29,31] Therefore, one of the benefits of the application of this type of structures in ECG electrodes relies on the improvement of the contact between the electrodes and the patient's skin, given the more distributed sensing area and the better conformation to the body's contours when compared to circular electrodes. Additionally, the self-similarity and infinite complexity of fractals increase the total sensing surface distribution on the skin with the same contact area, enhancing the comfort, accuracy, and reliability of ECG measurements. Moreover, it has been demonstrated that employing fractal designs in wearable sensors and actuators significantly enhances their sensitivity and expands the operation range of the sensor, resulting in faster and more stable responses.[22] Therefore, this technology provides consistent and reliable performance over time coupled with the mechanical flexibility required for wearable applications.[32]

This article focuses on the development of snowflake fractal-like electrode designs for ECG monitoring using a DLW fabrication process on a commercial polyimide to produce LIG. Inspired by dendritic, fernlike, and plate crystal structures, we created nine fractal-like designs based on the work presented by Bentley et al..[33] Note that although these fractal designs aim to replicate the aspect of fractal geometries, they do not feature the properties of idealized fractals from a mathematical perspective because of the real-world limitations and fabrication constrains. Therefore, they are frequently referred to as fractal-like structures. To make the electrodes as standard as possible, the electrodes are equipped with a snap terminal, thus avoiding the use of additional conductive inks and custom connections. The manufacturing process is described in detail, and the morphological and structural characteristics of the laser-induced material are analyzed using Scanning Electron Microscopy (SEM), Raman spectroscopy, and X-ray Photoelectron Spectroscopy (XPS). To evaluate the performance of the designs, ECG recordings were obtained from different volunteers and compared to reference measurements using Ag/AgCl commercial electrodes. The different ECG signals acquired were processed using a robust and accurate algorithm for the detection of QRS complexes intended for monitoring the heart rate,[34] and their performance was evaluated in terms of sensitivity, specificity, positive prediction, and accuracy.

2. Results and Discussion

2.1. Electrodes Fabrication

The technique used for the fabrication of the electrodes is DLW on the commercial polyimide Kapton HN film, on top of a paper sheet as depicted in **Figure 1**A. Due to the laser photothermal processing of the material, the weak molecular bonds of the precursor break by the photothermal effect and are released in the form of gases. This process modifies the physical and chemical properties of the material, resulting in a porous and conductive material commonly referred to as LIG.[17]

After the DLW process, each scribed electrode is cut with the laser, and a snap connector is then placed through the square terminal for its connection with the measurement unit, as presented in Figure 1C and described in the Experimental Section. The inclusion of the snap terminal, shown in Figure 1B, simplifies the manufacturing process by eliminating the need for silver ink application or soldering to attach a conductive cable as a connection terminal, as done in previously presented electrodes.[12,18–20] These aspects standardize the electrode design, and enhance the reliability of the connection with respect to previous designs, thus reducing the signal noise. In addition, with the adoption of silver-free electrodes, costly and environmentally harmful materials like silver chloride (AgCl) are no longer required, thus promoting a more sustainable and cost-effective alternative for biosignals acquisition. In Figure 1D, the commercial ECG measurements unit with the connection setup used in this work is shown along with our custom snap fractal-like electrodes.

Finally, a non-conductive lacquer is spread on both the metal snap and the terminal to ensure that they do not interfere with the measurements by coming into contact with the skin. It is worth mentioning that the presented electrodes are designed as dry electrodes, although it is also possible to apply electrolyte gel, if necessary, to improve the contact with the skin as in commercial electrodes.

The LIG-based electrodes are intended to be placed on the body according to Einthoven's triangle derivation I,[35] as depicted in Figure 1E. The LIG pattern is directly in contact with skin through the use of a standard cohesive medical bandage placed around the wrist of the volunteer, as presented in Figure 1F. In contrast to adhesive bandage, this one sticks only to itself, and not to skin or hair. For the evaluation of the performance of the different designs, the ECG signals are also acquired simultaneously using commercial electrodes, as presented in Figure 1F. For more detailed information, please refer to the Experimental Section.

2.2. Electrodes Design

In this work, we selected specific 2D snowflake patterns as the fractal geometry for our ECG electrodes, inspired from Bentley et al..[33] The selection criteria of each design were based on the level of symmetry, multiple ramifications, and compatibility with the 2D fabrication technique. The selected patterns are presented in **Figure 2** with their corresponding nomenclature and classification based on Magono et al..[36]

Two categories of designs were made: original shapes derived from real photographed snowflakes and stylized snowflakes where we optimized both symmetry and surface area. Due to the connection terminal, one ramification of the original snowflake structure was removed. Stylized snowflakes designs were considered to surpass the drawbacks of natural snowflakes patterns for this application. As seen in Figure 2, natural snowflakes (e.g., P1e-N1) possess more intricate and fine details compared with

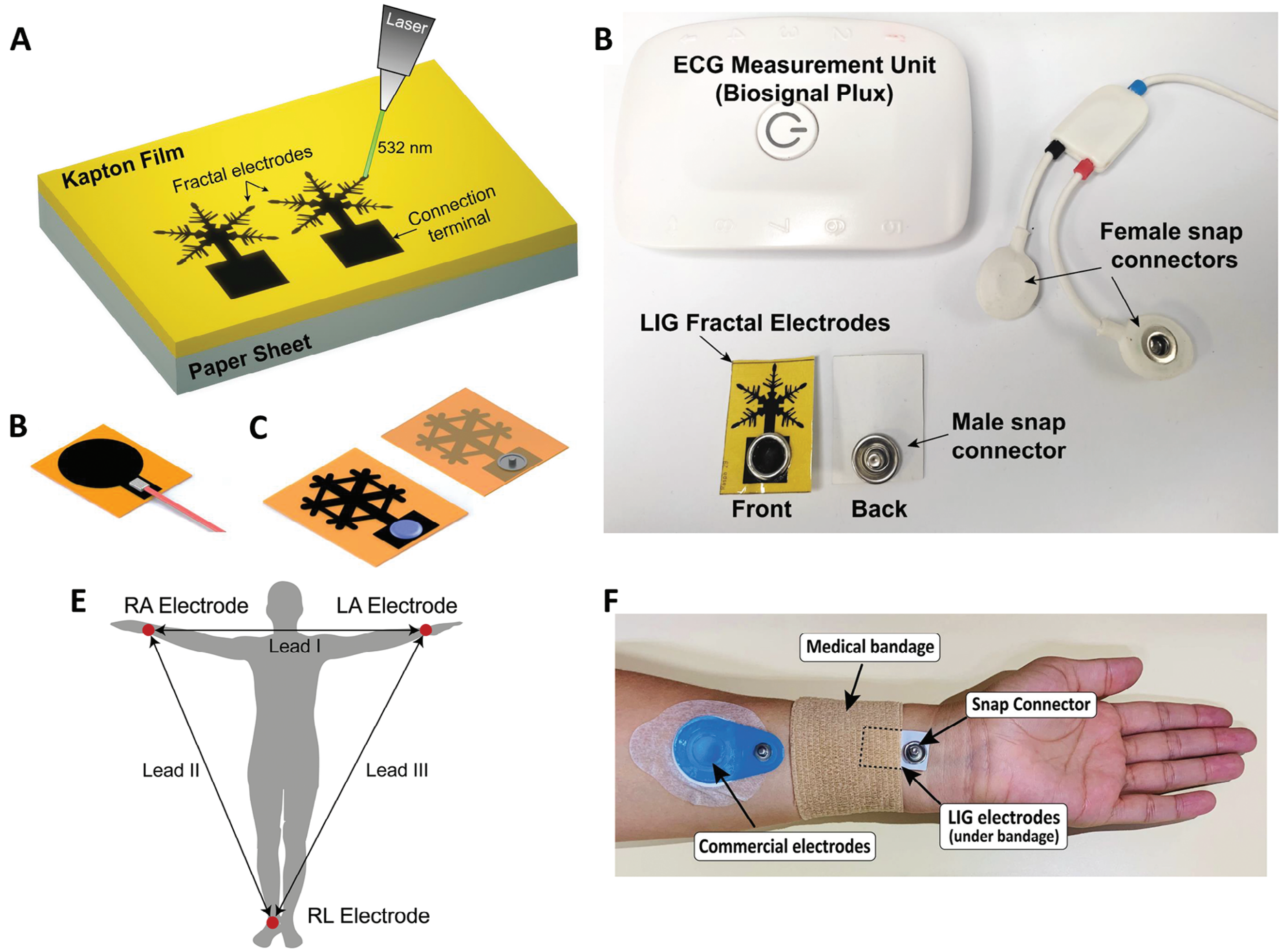

Figure 1. A) Schematic of the Direct Laser Writing method on polyimide film for fractal-like electrodes fabrication. B) Previous circular electrode with a cable glued with silver-based conductive ink for its connection to the acquisition equipment. C) Proposed fractal-like electrode with a standard snap terminal. D) Measurement equipment (Biosignals Plux acquisition unit and standard female snap connectors) together with one of the proposed fractal-like electrodes. E) Positioning of the electrodes on the body according to Einthoven's triangle derivation I. F) Electrodes placement on the wrist of the volunteer for the simultaneous ECG measurements.

the stylized electrodes. Since LIG is a resistive material, these fine details contribute to electrical losses, offering lower improvement over the stylized shapes, as experiments will demonstrate later. In addition, these fine details are more likely to get damaged as a consequence of the mechanical stress. Because of that, stylized geometries feature a compromise between the presence of fine details, which expand the acquisition surface and the signal potential measurement, and their thickness and robustness.

For comparison purposes, all designed electrodes have the same standard sensing area of 78.5 mm^2 (excluding the terminal). For that, we also incorporated a circular electrode with a diameter of 1 cm as a reference design. From a geometrical perspective, three key parameters were derived from the fractal-like designs: the active area (which remained constant at 78.5 mm^2 for all cases), the rectangular surface area (calculated as the rectangle that surrounds the pattern), and the perimeter of the pattern. These parameters, obtained through graphical analysis, are presented in **Table 1**. To determine the active area and perimeter of the designed electrodes, we counted the black pixels within the high-definition fractal-based image excluding the terminal. All patterns were designed to match the sensing area of the circular electrode with a diameter of 1 cm. As seen, all the fractal-like electrodes exhibit a more distributed sensing area, resulting in a higher effective surface area when compared to the circular reference design.

Table 1. Geometrical parameter (rectangular surface and perimeter) of each fractal-based design.

Name	Rectangular Surface [mm^2]	Perimeter [mm]	Name	Rectangular Surface [mm^2]	Perimeter [mm]
P1e-N1	185.2	243.9	P1e-S1	197.0	133.6
P1f-N1	199.5	233.0	P1f-S1	173.5	100.1
P1f-N2	266.8	194.9	P1f-S2	161.2	118.8
P2e-N1	151.1	72.5	P2e-S1	138.7	112.7
P2e-N2	170.4	114.0	Circ-1	100.0	31.4

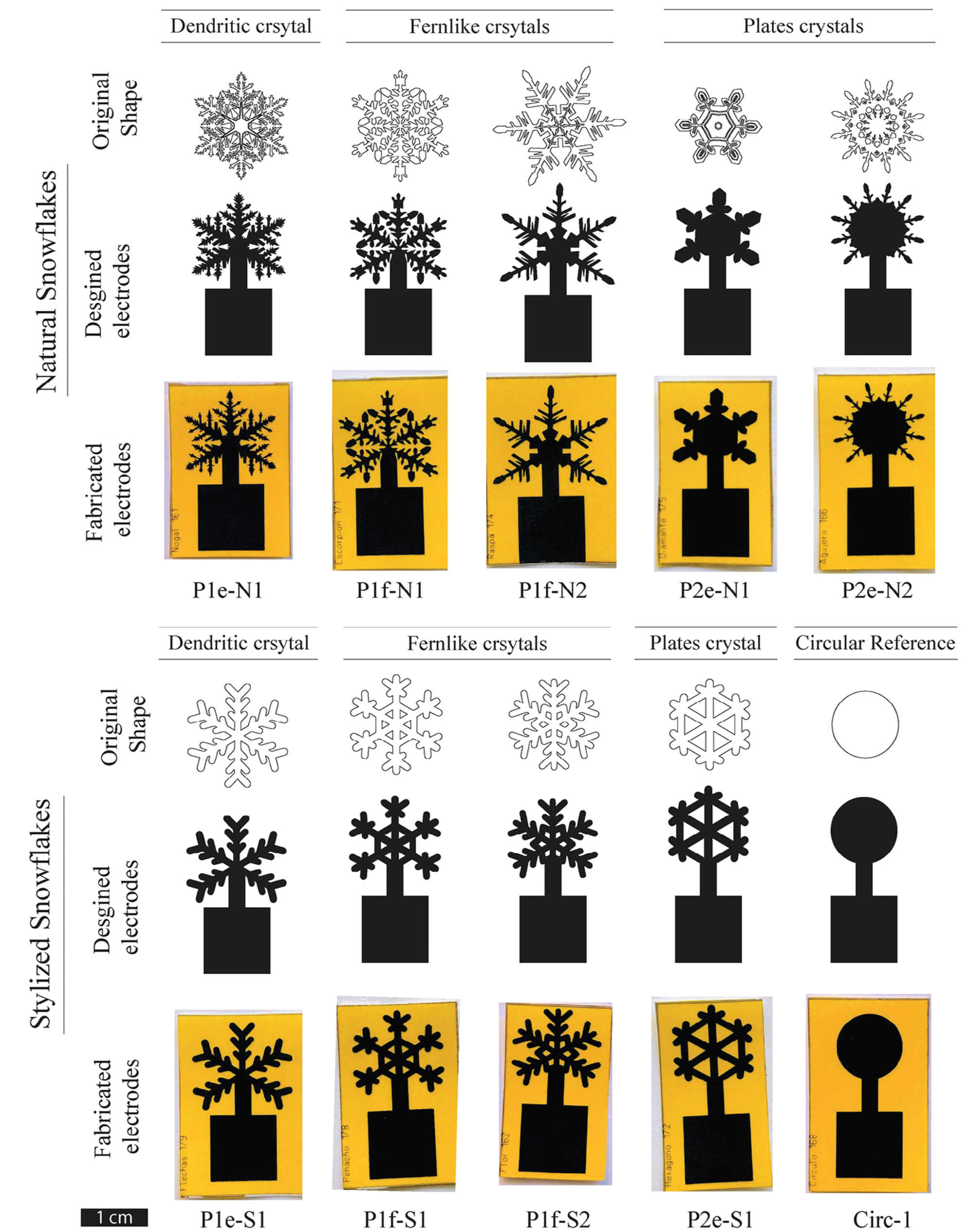

Figure 2. Schematic illustrations and real photographs of all the fabricated fractal-like electrodes.

2.3. Electrodes Structural Characterization

A SEM image of the laser processed surface is presented in **Figure 3A**. The surface presents horizontal trenches formed as a result of successive laser paths. Upon closer inspection of the inner image, the stacked layers and the porosity of the material become evident. The top of each trench measures ≈10 µm in thickness, while the spacing between two adjacent trenches is ≈50 µm. This 3D structure is small enough to fit with the morphology of the human skin, increasing the contact surface. Generally, the folds amplitude of the skin varies between 15 and 100 µm with lateral dimensions between 40 and 10^3 µm.[37,38] When the electrode is pressed onto the skin, the size and porosity of the electrode allow for a conformal contact, which contributes to improve the performance by minimizing motion artifacts and reducing background noise.[39,40]

The nature of the graphene-derived material formed during the fabrication process is confirmed through Raman spectroscopy, as shown in Figure 3B. The Raman spectrum of the resulting material reveals three prominent peaks located at 1350, 1580, and 2700 cm^{-1}, corresponding to the D, G, and 2D peaks, respectively. In particular, the I_{2D}/I_G ratio of 0.58 (usually >2 for single-layer pristine graphene) indicates the multilayer structure of the graphene-derived material,[41] while the ratio I_D/I_G ≈1 indicates the existence of defects in the sp^2-hybridized carbon crystalline structure.[42] Therefore, the observed Raman

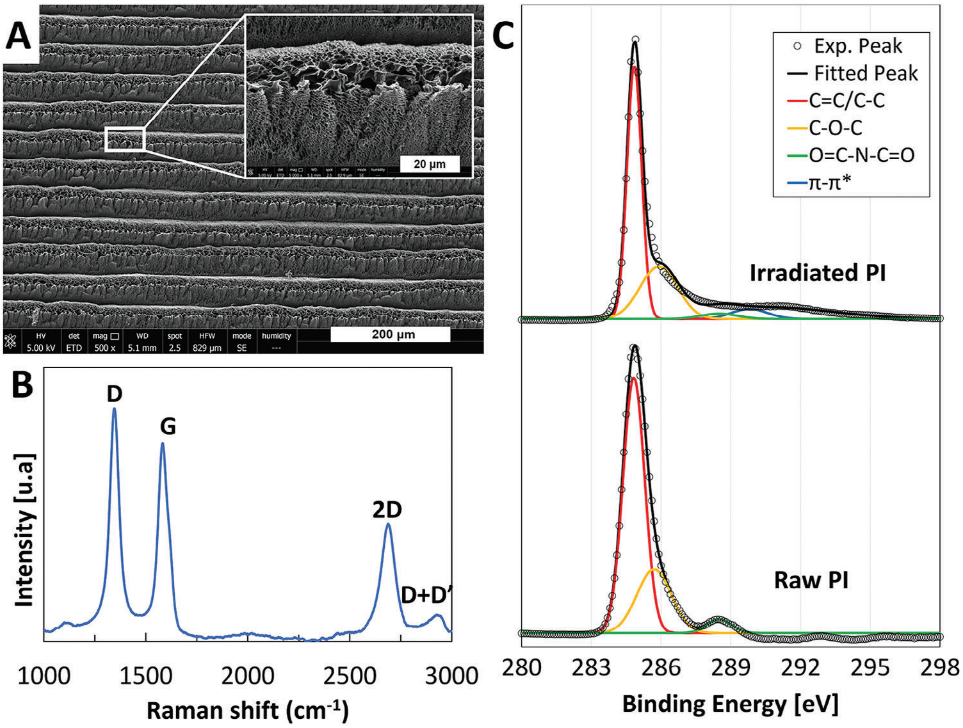

Figure 3. A) SEM image of the polyimide surface treated by the laser. B) Raman spectrum of the laser photothermal processed material with the identification of the D, G, and 2D peaks. C) Deconvolution of the C_{1s} peak for both processed and raw polyimide.

spectrum is characteristic of LIG and exhibits similarities to that of rGO.[17,43]

The chemical polyimide structure consists primarily of carbon (C), oxygen (O), and nitrogen (N). During the laser photothermal process, the laser's photothermal effect causes the radicals within the polymeric chain to break, leading to the release of gases such as CO_2, O_2, and N_2, among others.[44] The atomic concentration ratio of carbon to oxygen (C/O) increases significantly from 4.57 before irradiation to 47.79 after irradiation, representing an increase of more than ten times. Similarly, the carbon to nitrogen (C/N) ratio increases from 34.24 to 70.98 after the photothermal effect. The deconvolution of the C_{1s} peak is presented in Figure 3C, which reveals the presence of several components. The predominant peak corresponds to the sp^2 hybridization of carbon, observed at 284.8 eV. Additionally, there are two residual peaks detected at 286.0 and 288.5 eV, which can be attributed to C—O and C═O bonds, respectively.[45] After the photothermal process, both residual peaks decrease and the satellite π–π^* peak emerges. This peak indicates the presence of carbon atoms in sp^2 hybridization, thus confirming the graphitic nature of the induced material (since it is primarily observed graphite, graphene, and related carbon-based materials).[46,47] It arises from the excitation of the electrons of sp^2-hybridized bonds from a π orbital to a π^* antibonding orbital during the X-ray photon emission. In graphitic materials like LIG, the electrical conduction is caused by the presence of these sp^2 hybridized bonds with delocalized π electrons that can move freely across the plane, although it cannot be used as a direct measure of electrical conductivity.[48–50]

All these surface modifications lead to a great enhancement of the electrical conductivity with respect to the original polyimide precursor. The measured sheet resistances on the manufactured LIG electrodes are 35–40 Ω/sq., obtaining similar values to those reported in other works.[18,51]

2.4. ECG Electrode Performance

The evaluation of the performance of fractal-like LIG electrodes was conducted by comparing them to commercial electrodes as the reference. The goal was to extract parameters of interest, such as the identification of heartbeats, using the R-peaks of each QRS complex as a reference point. An example of the raw signals acquired simultaneously using both types of electrodes, CH1 using LIG fractal-like electrode (P2e-N2) and CH2 using a commercial electrode, is shown in **Figure** 4A. As detailed in the Experimental Section, prior to the identification and classification of the QRS complexes, the algorithm applies a denoising step based on the wavelet transform.[34] As depicted in Figure 4B, on the one hand, this initial stage removes the low-frequency noise and wandering of the signal (thus centering the signal in 0 V) and, on the other hand, it also filters the high frequency components, smoothing the signal and reducing the electrical noise at 50 Hz. After the denoising step, the clustering algorithm identifies the different peaks that compose the signal and classifies them into two distinct groups: R-peaks (from the QRS complex) and other waves. For that, the relative amplitude of the peaks and the time interval between them are used as features for the classification. For instance, Figure 4C shows the identification of the R-peaks for one of the acquired signals, where the frequency of the peaks is used to extract the heart rate over time.

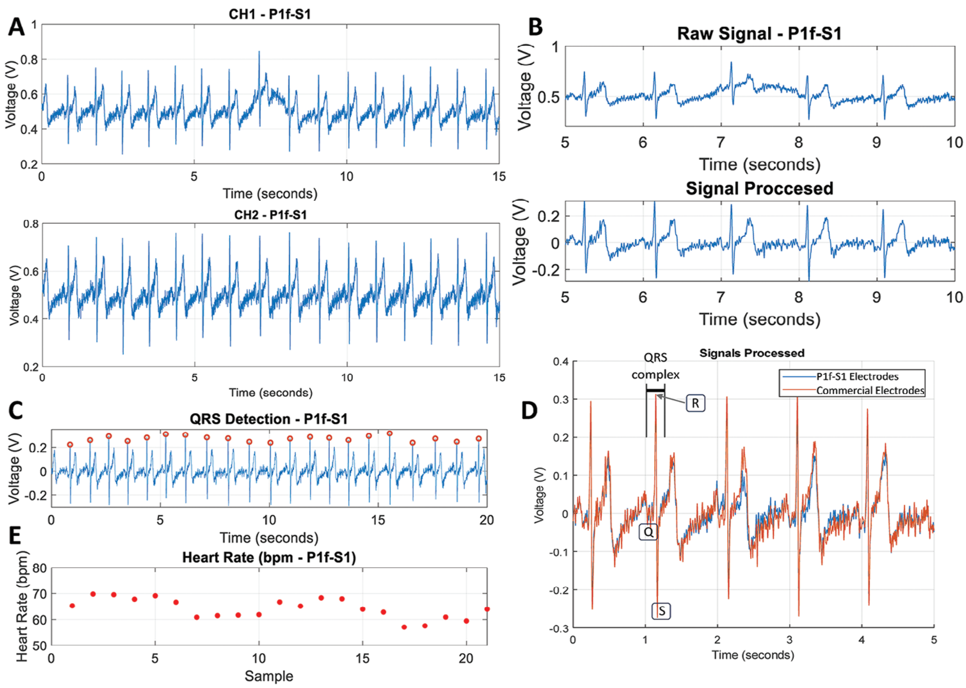

Figure 4. A) Raw ECG signals are acquired simultaneously using two channels of the acquisition equipment corresponding to the fractal-like LIG electrode P1f-S1 (CH1) and commercial electrode (CH2). B) ECG signal from electrode P1f-S1 before (top) and after (bottom) the denoising stage. C) R-peaks identification on the ECG. D) Comparison of the two processed signals acquired from LIG electrode P1f-S1 (orange) and commercial electrode (blue). E) Instantaneous heart rate extracted from the R-peak detection of the LIG electrode P1f-S1 ECG signal.

The signals acquired simultaneously for both fractal-like and commercial electrodes are processed using the same conditions for the identification of the R-peaks detailed in the Experimental Section (Figure 4D). The higher the crest factor of the signals (ratio between the amplitude of the R peak and the RMS value of the signal[52]), the better the classification. In the case of the signals of Figure 4D, this value is 31.07 dB for the LIG P1f-S1 electrodes and 28.64 dB for the commercial ones, thereby demonstrating a less noisy acquisition capability. Then, a comparison based on the true/false positives and negatives is done to extract the different figures of merit presented in Equations 1–4: sensitivity (Se), specificity (Sp), positive predictivity (PP), and accuracy (A).

Detailed results of the performance of the LIG electrodes with respect to the commercial electrodes are presented in the **Figures 5** and **6**. In particular, **Figure 5** shows the comparison of the LIG reference electrode (circular, Figure 5A) and the electrodes with "natural snowflake" fractal-based designs (Figure 5B–F). The results for these electrodes demonstrate a similar performance in most cases, being all different figures of merit higher than 95% in all cases. However, note that the sensitivity of the natural fractal-based designs (P1e-N1 98.22% Se, P1f-N1 99.60% Se, P1f-N2 98.62% Se, P2e-N1 96.79% Se, P2e-N2 97.21% Se) outperforms the sensitivity of both circular electrode (96.58%) and commercial electrodes, while the rest of parameters are very similar for all of them.

Furthermore, as detailed in Section 2.2, some of the natural snowflake's structures were modified to obtain optimized snowflake fractal-like electrodes for this purpose. **Figure 6** provides the experimental results for the performance parameters of the fractal-like stylized snowflakes electrodes, which exhibit notable enhancements when compared with both the natural snowflakes and circular electrodes. These improvements are evident in the increased values of sensitivity, specificity, positive prediction, and accuracy, all of which surpass 98%.

The comparative analysis between all the flexible LIG electrodes aimed at identifying the electrode with better performance is depicted in **Figure 7**. As observed, the stylized geometries not only result in higher average values for the different figures of merit, but also exhibit less variability among subjects. This enhanced performance and reduced variability is attributed to the thicker and more robust design, resulting in a better trade-off between improving contact robustness and reducing electrical losses. Additionally, the more uniformly distributed electrical surface accounts for the superior performance of stylized designs characterized by interconnected patterns (P1f-S1, P1f-S2, and P2e-S1) compared to designs based on independent branches (P1e-S1). Specifically, the P2e-S1 design, featuring a hexagonal plate snowflake pattern, demonstrates exceptional characteristics across all figures of merit, including sensitivity (99.60%), specificity (99.99%), positive predictive value (99.62%), and overall accuracy (99.93%).

In general, all these results demonstrate significant advancements compared to previous research on flexible dry LIG electrodes.[19–21] Such improvements can be attributed not only to the inclusion of a standardized and reliable snap connection, simplifying connectivity, and reducing fabrication steps, but also to the superior signal acquisition quality introduced by the utilization of some optimized fractal-like structures, as demonstrated when comparing the results with those achieved for the CIRC-1 reference electrode.

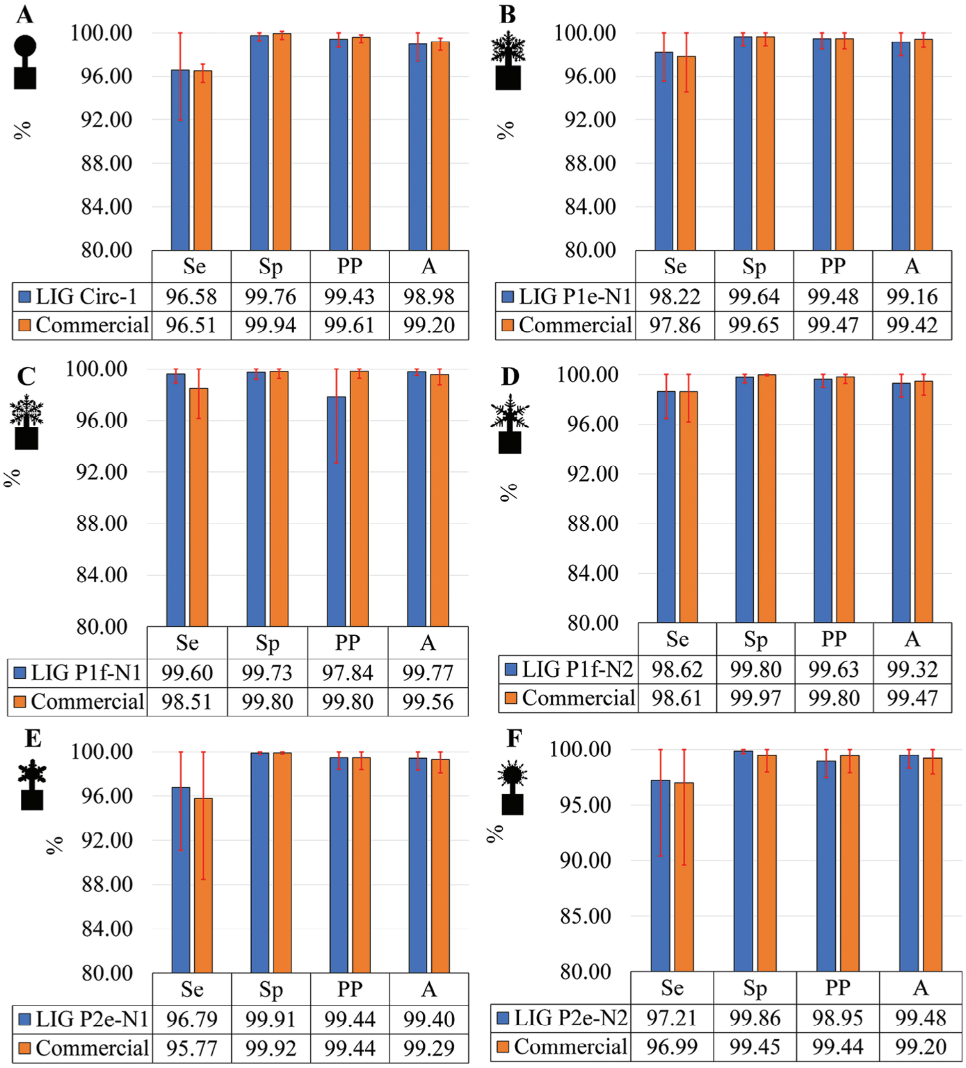

Figure 5. Comparison of the different figures of merit (Se: Sensitivity, Sp: Specificity, PP: Positive Preduction, A: Accuracy) the circular reference electrode and natural snowflake LIG patterns with respect to the commercial electrodes extracted from the measurement of the eight subjects: A) CIRC-1, B) P1e-N1, C) P1f-N1, D) P1f-N2, E) P2e-N1, F) P2e-N2.

3. Conclusion

This work presents the fabrication and surface area optimization of ECG electrodes using laser-induced graphene (LIG). In particular, we characterized electrodes with fractal-based geometries inspired by both natural and optimized snowflake patterns, which are laser-scribed directly on the surface of a commercial flexible polyimide. Ten different electrodes were designed with the same surface area, including five natural snowflakes, four optimized snowflakes, and a circular electrode used as a reference. To evaluate the performance of the different designs, we compared these electrodes together with commercial electrodes (Ag/AgCl) in terms of sensitivity, specificity, positive prediction, and accuracy. For that, we conducted simultaneous measurements using two different channels of a portable electronic electrocardiography device and analyzed the data with an algorithm for QRS complexes detection, including a previous wavelet-based preprocessing for denoising. The results show that the fractal-like electrodes presented in this work allow the enhancement of the acquisition quality of ECG signals with respect to traditional circular designs without any additional cost or extra fabrication step. In addition, it is also demonstrated that the more distributed geometries with reduced intricacies and increased thickness in the printed lines effectively mitigates resistive losses and increase robustness to skin contact, hence offering the best performance with sensitivity, specificity, positive prediction, and accuracy values above 99.6% for the QRS complex detection.

4. Experimental Section

Materials: The raw material for the synthesis of the LIG was the commercial Kapton polyimide film from 3D-Drucker-Filament. The total thickness of the film was 60 µm, with 25 µm of polyimide and 35 µm of adhesive. To ensure a smooth surface, the film was stretched and pressed to

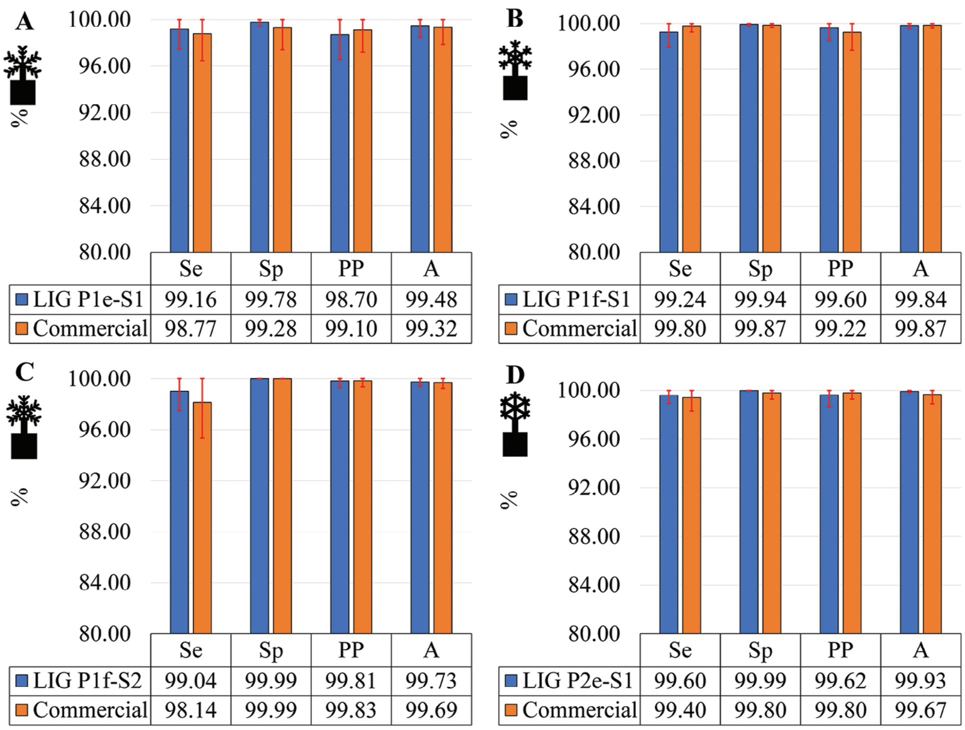

Figure 6. Comparison of the different figures of merit (Se: Sensitivity, Sp: Specificity, PP: Positive Preduction, A: Accuracy) for the optimized snowflake LIG patterns with respect to the commercial electrodes extracted from the measurements of the eight subjects: A) P1e-S1, B) P1f-S1, C) P1f-S2, D) P2e-S1.

eliminate any undulations or bubbles on top of a 90 µm thick A4 white paper sheet. The paper layer provides consistency to the electrodes, preventing the deformation of the polyimide as a consequence of the heat generated during the laser photothermal process and facilitating the placement of the snap connector. The surface of the polyimide was cleaned afterward with isopropyl alcohol from RS Pro©. Commercial silver/silver chloride (Ag/AgCl) ECG electrodes from Ambu A/S, specifically the Ambu BlueSensor VL:VL-00-S/25 electrodes, were used for comparison purposes. The electrical connection to the electrode was performed using stainless steel fastener snaps from RERI. These snaps have a diameter of 10 mm and consist of a hollow prong eyelet on the front of the electrode's terminal and a male snap on the back.

Material Characterization: The microstructure of laser-induced material was analyzed using a Scanning Electron Microscope (SEM) NVision40 from Carl Zeiss (Oberkochen, Germany) at an extraction and acceleration voltage of 5 kV, otherwise noted.

A dispersive micro-Raman spectrometer JASCO NRS-5100 (Easton, PA, USA) with a green diode (Elforlight G4-30; Nd:YAG, l = 532 nm) as excitation source was used for the Raman spectra acquisition. The sampling parameters were set to three accumulations with 30 s of exposure time. The X-ray Photoelectron Spectroscopy (XPS) was carried out on a Kratos Axis Ultra-DLD (Manchester, UK), using an X-ray (Al Kα hv = 1486.6 eV) power of 450 W in a vacuum chamber where the pressure was kept below 10^{-10} Torr.

For the electrical characterization, the sheet resistance was measured applying the method "In-Line Four-Point Probe with the Dual-Configuration"[53] using the Universal Four-Probe station from Jandel and the Source Meter Unit (SMU) B2902A from Keysight.

Electrode Fabrication: The adhesive polyimide thin film was placed on top of an A4 paper sheet used as a substrate to improve its machinability. Then, the surface was cleaned using isopropyl alcohol and dried for 1 min prior to the laser photothermal processing at ambient conditions. The laser used was a PowerLine E-12-532 from Coherent, a galvanometric laser with a wavelength of 532 nm with a laser resolution of 50 µm. The adjustable parameters were set to: optical power 0.8 W, scan speed of the beam 40 mm s^{-1}, frequency 50 kHz, and focus point 270 mm. This laser fluence allows for the lowest sheet resistance without damaging neither the polyimide film substrate nor the paper below.[54] A fume extractor was located nearby to absorb the smoke generated during the laser photothermal process. After the laser-scribing of the LIG electrode, it was equipped with a standard snap male connector. As done for snap buttons on fabric, the connector was placed by sandwiching the electrode terminal between the two metallic pieces of the snap connector (Figure 1B). For that, the prongs of one piece were inserted through the substrate and then secured into the other piece by using a standard pair of snap pliers. This process ensures a robust electrical contact with the LIG layer without the need for pre-existing cuts or holes. Finally, an insulator lacquer was applied to the terminal to avoid the contact with the patient's skin.

Electrodes Performance Characterization: The acquisition of the ECG signals was performed using a Biosignals Researcher Kit portable equipment with two three-lead local differential ECG electrodes (from PLUX wireless biosignals S.A.). The acquired signals were sent to a computer via Bluetooth using the software OpenSignals (r)evolution (from PLUX wireless Biosignals S.A.) and post-processed in Matlab.

A total of eight healthy volunteers with an age range from 20 to 30 years old and a weight range from 45 to 80 kg participated in this study. All experiments were conducted in accordance with the Declaration of Helsinki. All human participants took part in the experiments voluntarily with informed written consent. No further ethical approval was required for this study. The measurements were performed using two channels (CH1-CH2) on the measuring device: CH1 for the LIG electrodes and CH2 for the commercial electrodes. The signals were acquired simultaneously by positioning the electrodes on the body according to Einthoven's triangle derivation I,[35] see Figure 1E. Both pairs of electrodes (LIG and commercial) were placed on the wrists of the volunteer (left arm positive, right arm negative). Finally, a commercial reference electrode was positioned on the

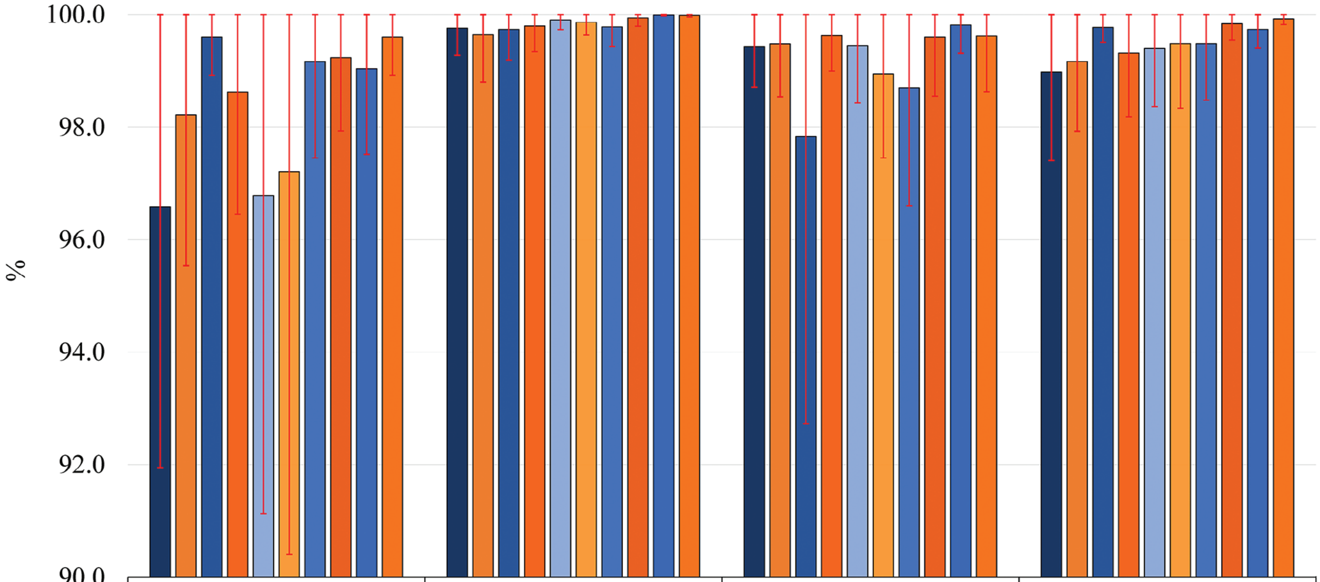

	Sensitivity (Se)	Specificity (Sp)	Positive Prediction (PP)	Accuracy (A)
CIRC-1	96.58	99.76	99.43	98.98
P1e-N1	98.22	99.64	99.48	99.16
P1f-N1	99.60	99.73	97.84	99.77
P1f-N2	98.62	99.80	99.63	99.32
P2e-N1	96.79	99.91	99.44	99.40
P2e-N2	97.21	99.86	98.95	99.48
P1e-S1	99.16	99.78	98.70	99.48
P1f-S1	99.24	99.94	99.60	99.84
P1f-S2	99.04	99.99	99.81	99.73
P2e-S1	99.60	99.99	99.62	99.93

Figure 7. Comparison of the figures of merit extracted from the measurements of the eight subjects for the different LIG electrodes: circular (reference) and both natural and stylized snowflakes patterns.

left ankle. All ECG signals were recorded for at least 2 min in the software OpenSignal and analyzed in the Matlab algorithm for 60 s.

The processing of the ECG signals was performed using a modified version of the clustering-based algorithm proposed by Castillo et al. to both filter the signal and detect the QRS complexes.[55] This algorithm, designed to be implemented in portable devices, uses the discrete wavelet transform (DWT) to remove the low-frequency components of the signal (0–1 Hz) and filter the higher frequencies (>31.25 Hz) while maintaining the frequency range of interest unchanged.[56] Once the signal was filtered, the second stage of the algorithm applies a clustering method to classify the amplitude of the local maxima followed by a local minimum into two clusters, distinguishing QRS complexes from noise and other waves (instead of three cluster classification as was done in the original algorithm proposed by Castillo et al. for fetal ECG[55]). This technique proposed by Castillo et al. and the modified version used in this paper are more effective in identifying R peaks compared to traditional threshold-based algorithms. It can accurately detect QRS complexes with varying amplitudes between the RS peaks and avoid identifying T waves with large amplitude as R peaks, reducing false negatives and false positives.[20]

The different performance parameters were calculated as follows[57]:

1. Sensitivity (*Se*).

$$Se\ (\%) = \frac{TP}{TP + FN} \times 100 \tag{1}$$

2. Specificity (*Sp*).

$$Sp\ (\%) = \frac{TN}{TN + FP} \times 100 \tag{2}$$

3. Positive predictivity (*PP*).

$$PP\ (\%) = \frac{TP}{TP + FP} \times 100 \tag{3}$$

4. Accuracy (*A*).

$$A\ (\%) = \frac{TP + TN}{TP + TN + FN + FP} \times 100 \tag{4}$$

where TP (true positive) represents the correct detected peak, the FP (false positive) represents the falsely identified peak, and FN (false negative) represents the misidentified peak as other noise.

Acknowledgements

This work was supported by Grant PID2020-117344RB-I00 funded by MCIN/AEI 10.13039/501100011033. Further support was obtained from the FEDER/Junta de Andalucía-Consejería de Transformación

Económica, Industria, Conocimiento y Universidades Project P20_00265 and Project BRNM-680-UGR20; Project TED2021-129949A-I00 funded by MCIN/AEI/10.13039/501100011033 and by European Union NextGenerationEU/PRTR. In addition, this work was also supported by the Junta de Andalucía – Consejería de Universidad, Investigación e Innovación through the project ProyExcel_00268 as well as by the Spanish Ministry of Sciences and Innovation through the Ramón y Cajal fellow RYC2019-027457-I and the pre-doctoral grant PRE2021-096886.

Conflict of Interest

The authors declare no conflict of interest.

Data Availability Statement

The data that support the findings of this study are available from the corresponding author upon reasonable request.

Keywords

dry electrodes, electrocardiogram, flexible electronics, fractal geometry, laser-induced graphene

Received: November 7, 2023
Revised: December 27, 2023
Published online:

[1] Y. J. Hong, H. Jeong, K. W. Cho, N. Lu, D.-H. Kim, *Adv. Funct. Mater.* **2019**, *29*, 1808247.
[2] D. De Bacquer, G. De Backer, M. Kornitzer, H. Blackburn, *Heart* **1998**, *80*, 570.
[3] C. Wang, K. Xia, H. Wang, X. Liang, Z. Yin, Y. Zhang, *Adv. Mater.* **2019**, *31*, 1801072.
[4] D. Corzo, G. Tostado-Blázquez, D. Baran, *Front. Electron.* **2020**, *1*, 594003.
[5] M. M. Rodgers, V. M. Pai, R. S. Conroy, *IEEE Sens. J.* **2014**, *15*, 3119.
[6] J. C. Yeo, C. T. Lim, *Microsyst. Nanoeng.* **2016**, *2*, 16043.
[7] A. Portelli, S. Nasuto, *Biosensors* **2017**, *7*, 2.
[8] A. Searle, L. Kirkup, *Physiol. Meas.* **2000**, *21*, 271.
[9] H. Halvaei, L. Sörnmo, M. Stridh, *Sensors* **2021**, *21*, 5548.
[10] N. Meziane, J. G. Webster, M. Attari, A. J. Nimunkar, *Physiol. Meas.* **2013**, *34*, R47.
[11] Y. Fu, J. Zhao, Y. Dong, X. Wang, *Sensors* **2020**, *20*, 3651.
[12] C. Lou, R. Li, Z. Li, T. Liang, Z. Wei, M. Run, X. Yan, X. Liu, *Sensors* **2016**, *16*, 1833.
[13] T.-R. Cui, D. Li, X.-R. Huang, A.-Z. Yan, Y. Dong, J.-D. Xu, Y.-Z. Guo, Y. Wang, Z.-K. Chen, W.-C. Shao, Z.-Y. Tang, H. Tian, Y. Yang, T.-L. Ren, *Appl. Sci.* **2022**, *12*, 4526.
[14] A. Kolanowska, A. P. Herman, R. G. Jedrysiak, S. Boncel, *RSC Adv.* **2021**, *11*, 3020.
[15] H.-C. Jung, J.-H. Moon, D.-H. Baek, J.-H. Lee, Y.-Y. Choi, J.-S. Hong, S.-H. Lee, *IEEE Trans. Biomed. Eng.* **2012**, *59*, 1472.
[16] P. S. Das, M. F. Hossain, J. Y. Park, *Microelectron. Eng.* **2017**, *180*, 45.
[17] J. Lin, Z. Peng, Y. Liu, F. Ruiz-Zepeda, R. Ye, E. L. Samuel, M. J. Yacaman, B. I. Yakobson, J. M. Tour, *Nat. Commun.* **2014**, *5*, 5714.
[18] M. A. Zahed, P. S. Das, P. Maharjan, S. C. Barman, M. Sharifuzzaman, S. H. Yoon, J. Y. Park, *Carbon* **2020**, *165*, 26.
[19] V. Toral, E. Castillo, A. Albretch, F. J. Romero, A. Garcia, N. Rodriguez, P. Lugli, D. P. Morales, A. Rivadeneyra, *IEEE Access* **2020**, *8*, 127789.
[20] F. J. Romero, E. Castillo, A. Rivadeneyra, A. Toral-Lopez, M. Becherer, F. G. Ruiz, N. Rodriguez, D. P. Morales, *npj Flexible Electron.* **2019**, *3*, 12.
[21] T.-R. Cui, D. Li, X.-R. Huang, A.-Z. Yan, Y. Dong, J.-D. Xu, Y.-Z. Guo, Y. Wang, Z.-K. Chen, W.-C. Shao, Z.-Y. Tang, H. Tian, Y. Yang, T.-L. Ren, *Appl. Sci.* **2022**, *12*, 4526.
[22] J. A. Fan, W.-H. Yeo, Y. Su, Y. Hattori, W. Lee, S.-Y. Jung, Y. Zhang, Z. Liu, H. Cheng, L. Falgout, M. Bajema, T. Coleman, D. Gregoire, R. J. Larsen, Y. Huang, J. A. Rogers, *Nat. Commun.* **2014**, *5*, 3266.
[23] W. J. Watterson, R. D. Montgomery, R. P. Taylor, *Sci. Rep.* **2017**, *7*, 6717.
[24] F. Tian, A. Jiang, T. Yang, J. Qian, R. Liu, M. Jiang, *IEEE Sens. J.* **2021**, *21*, 14587.
[25] Anguera, Andújar, Jayasinghe, Chakravarthy, Chowdary, Pijoan, Ali, Cattani, *Fractal Fract.* **2020**, *4*, 3.
[26] I. Reljin, B. Reljin, *Arch. Oncol.* **2002**, *10*, 283.
[27] K. Falconer, *Fractal Geometry: Mathematical Foundations and Applications*, 2nd ed., John Wiley & Sons, Hoboken, NJ, USA, **2004**.
[28] B. Mandelbrot, *Science* **1967**, *156*, 636.
[29] J. Nittmann, H. E. Stanley, *J. Phys. A Math. Theor.* **1987**, *20*, L1185.
[30] J. Tyynelä, J. Leinonen, D. Moisseev, T. Nousiainen, *J. Atmos. Ocean. Technol.* **2011**, *28*, 1365.
[31] S. R. Fassnacht, J. Innes, N. Kouwen, E. D. Soulis, *Hydrol. Process.* **1999**, *13*, 2945.
[32] C. Vu, T. Truong, J. Kim, *Mater. Today Phys.* **2022**, 100795.
[33] W. A. Bentley, W. J. Humphreys, *Snow Crystals, Courier Corporation*, Dover Publication, Mineola, NY, USA **2013**.
[34] E. Castillo, D. P. Morales, A. García, L. Parrilla, V. U. Ruiz, J. A. Álvarez-Bermejo, *PLoS One* **2018**, *13*, e0199308.
[35] S. S. Barold, *Card. Electrophysiol. Rev.* **2003**, *7*, 99.
[36] C. Magono, C. W. Lee, *J. Fac. Sci. Hokkaido Univ. Ser. 7, Geophys* **1966**, *2*, 321.
[37] L. Tchvialeva, H. Zeng, I. Markhvida, D. I. McLean, H. Lui, T. K. Lee, *New Developments in Biomedical Engineering*, IntechOpen Limited, London, UK **2010**, 341.
[38] K.-P. Wilhelm, P. Elsner, E. Berardesca, H. I. Maibach, *Bioengineering of the Skin: Skin Imaging & Analysis*, 2nd ed., CRC Press, Boca Raton, FL, USA **2006**.
[39] A. Dallinger, K. Keller, H. Fitzek, F. Greco, *ACS Appl. Mater. Interfaces* **2020**, *12*, 19855.
[40] J.-W. Jeong, W.-H. Yeo, A. Akhtar, J. J. S. Norton, Y.-J. Kwack, S. Li, S.-Y. Jung, Y. Su, W. Lee, J. Xia, H. Cheng, Y. Huang, W.-S. Choi, T. Bretl, J. A. Rogers, *Adv. Mater.* **2013**, *25*, 6839.
[41] Y. Hao, Y. Wang, L. Wang, Z. Ni, Z. Wang, R. Wang, C. K. Koo, Z. Shen, J. T. L. Thong, *Small* **2010**, *6*, 195.
[42] J.-B. Wu, M.-L. Lin, X. Cong, H.-N. Liu, P.-H. Tan, *Chem. Soc. Rev.* **2018**, *47*, 1822.
[43] F. J. Romero, A. Rivadeneyra, V. Toral, E. Castillo, F. García-Ruiz, D. P. Morales, N. Rodriguez, *Sens. Actuators, A* **2018**, *274*, 148.
[44] M. Inagaki, S. Harada, T. Sato, T. Nakajima, Y. Horino, K. Morita, *Carbon* **1989**, *27*, 253.
[45] N. Dwivedi, R. J. Yeo, N. Satyanarayana, S. Kundu, S. Tripathy, C. Bhatia, *Sci. Rep.* **2015**, *5*, 7772.
[46] Y. Lu, Y. Jiang, H. Wu, W. Chen, *Electrochim. Acta* **2015**, *156*, 267.
[47] Q. Yuan, C.-T. Lin, K. W. A. Chee, *APL Mater.* **2019**, *7*, 030901.
[48] K. Gross, J. J. P. Barragán, S. Sangiao, J. M. De Teresa, L. Lajaunie, R. Arenal, H. A. Calderón, P. Prieto, *Nanotechnology* **2016**, *27*, 365708.
[49] D. D. L. Chung *Carbon Materials: Science and Applications*, World Scientific, Singapore **2019**.
[50] D. Pantea, H. Darmstadt, S. Kaliaguine, C. Roy, *Appl. Surf. Sci.* **2003**, *217*, 181.
[51] J. Yang, K. Zhang, J. Yu, S. Zhang, L. He, S. Wu, C. Liu, Y. Deng, *Adv. Mater. Technol.* **2021**, *6*, 2100262.
[52] S. Takamatsu, T. Lonjaret, D. Crisp, J.-M. Badier, G. G. Malliaras, E. Ismailova, *Sci. Rep.* **2015**, *5*, 15003.

[53] *Am. Soc. Test. Mater.* **1997**, *10*, 13.
[54] Y. Houeix, F. J. Romero, C. L. Moraila, A. Rivadeneyra, N. Rodriguez, D. P. Morales, A. Salinas-Castillo, *Appl. Surf. Sci.* **2023**, *634*, 157629.
[55] E. Castillo, D. P. Morales, A. García, L. Parrilla, V. U. Ruiz, J. A. Álvarez-Bermejo, *PLoS One* **2018**, *13*, e0199308.
[56] E. Castillo, D. P. Morales, A. García, F. Martínez-Martí, L. Parrilla, A. J. Palma, *J. Appl. Math.* **2013**, *2013*, 763903.
[57] U. Satija, B. Ramkumar, M. S. Manikandan, *Biocybern. Biomed. Eng.* **2018**, *38*, 54.

